



Synthesis of $\text{Ru}_{0.58}\text{In}_{0.42}\text{O}_y \cdot n\text{H}_2\text{O}$ nanoparticles dispersed onto poly(sodium-4-styrene sulfonate)-functionalized multi-walled carbon nanotubes and their application for electrochemical capacitors

Changzhou Yuan^{a,b,*}, Linrui Hou^a, Long Yang^a, Diankai Li^a, Jie Tan^a, Laifa Shen^b, Fang Zhang^b, Xiaogang Zhang^{b,*}

^a Anhui Key Laboratory of Metal Materials and Processing, School of Materials Science & Engineering, Anhui University of Technology, Maanshan 243002, PR China

^b College of Material Science & Engineering, Nanjing University of Aeronautics & Astronautics, Nanjing 210016, PR China

ARTICLE INFO

Article history:

Received 5 September 2010

Accepted 28 October 2010

Available online 2 November 2010

Keywords:

Functionalized multi-walled carbon nanotubes

$\text{Ru}_{0.58}\text{In}_{0.42}\text{O}_y \cdot n\text{H}_2\text{O}$ nanoparticles

Poly(sodium-4-styrene sulfonate)

Monodispersion

Electrochemical capacitance

ABSTRACT

In this work, poly(sodium-4-styrene sulfonate) (PSS)-functionalized multi-walled carbon nanotubes (FMWCNTs) were first synthesized via a polymer-assisted technique. Then, $\text{Ru}_{0.58}\text{In}_{0.42}\text{O}_y \cdot n\text{H}_2\text{O}$ nanoparticles (NPs) were mono-dispersed onto the FMWCNTs surfaces under mild hydrothermal condition. Here, PSS with negative charge serves as a bifunctional molecule both for solubilizing and dispersing MWCNTs into aqueous solution and for tethering Ru^{3+} and In^{3+} to facilitate the good dispersion of $\text{Ru}_{1-x}\text{In}_x\text{O}_y \cdot n\text{H}_2\text{O}$ NPs onto their surfaces. The good dispersion of $\text{Ru}_{0.58}\text{In}_{0.42}\text{O}_y \cdot n\text{H}_2\text{O}$ NPs onto FMWCNTs makes OH^- ions and electrons easily contact these NPs with abundant electroactive sites, which results in a large specific capacitance (SC) of 319 F g^{-1} for the nanocomposites. Moreover, a symmetric electrochemical capacitor (EC) is constructed by using the nanocomposites as electrodes and delivers large specific energy density of 18.1 Wh kg^{-1} , desirable power property of 1302 W kg^{-1} , high electrochemical reversibility and good SC retention of 84.7%.

© 2010 Elsevier Inc. All rights reserved.

1. Introduction

Recently, carbon-based electroactive materials for electrochemical capacitors (ECs) have drawn much attention due to their high specific surface area and porous nature [1–4]. Particularly, multi-walled carbon nanotubes (MWCNTs), as one of the attractive carbon materials, have been recognized [5,6] widely for ECs application, considering their unique structural and electronic properties, such as high chemical stability, low mass density, low resistivity, narrow distribution of mesopore sizes, and large surface area to weight ratio as well as the ability to form a three-dimensional conducting matrix. However, their specific capacitances (SCs) are commonly very low. Hence, considerable efforts have been made to improve the SCs of MWCNTs-based electrode materials by various methods, such as chemical activation [7], and modification by using electronic conducting polymers (ECPs) [8–10] and/or transition-metal oxides with typical pseudocapacitive properties [11–16].

Obviously, the combination of an electric double layer system and a pseudocapacitive system could be a better candidate for an

EC with higher energy density and power property, because such hybrid can both utilize the fast and reversible pseudocapacitance and the indefinitely reversible double-layer capacitance at the electrode–electrolyte interfaces [5]. However, owing to the poor stability of ECPs [8–10], transition metal oxides owning better electrochemical stability and higher SCs have been extensively studied and expected to offer the enhanced capacitive performance. Among various transition metal oxides, Ru-based oxides doped with homovalent and/or heterovalent substitution (donated as $\text{Ru}_x\text{Me}_{1-x}\text{O}_y$, where Me represents Co [17,18], Ni [19], Sn [20,21], Ti [22], V [23,24], Cr [25,26], Zr [27], Ce [28], etc.) have been recognized as the most promising candidates for ECs, due to their larger SCs and better electrochemical stability. Hitherto, the synthesis of Ru-based oxides/MWCNTs nanocomposites with a uniform structure, unfortunately, has been a great challenge yet. Therefore, a facile and effective method to synthesize Ru-based oxides/MWCNTs composites with uniform nanostructure and good electrochemical capacitance is highly desired.

Recently, polymer-assisted technique has been envisaged to be a facile, cost-effective, and general approach to synthesis of metal oxides/MWCNTs nanocomposites [11–13,29]. Poly(sodium-4-styrene sulfonate) (PSS) cannot only solubilize and disperse MWCNTs well into the aqueous solution but also noncovalently functionalize MWCNTs through a polymer-wrapping mechanism [11–13,29–31]. As a consequence, the PSS-functionalized MWCNTs (FMWCNTs)

* Corresponding authors. Address: Anhui Key Laboratory of Metal Materials and Processing, School of Materials Science & Engineering, Anhui University of Technology, Maanshan 243002, PR China (C. Yuan). Fax: +86 025 52112626.

E-mail addresses: ayuancz@163.com (C. Yuan), azhangxg@163.com (X. Zhang).

would be dispersed well in an aqueous solution and create much more electroactive sites tethering metal ions with positive charge for subsequent formation of metal oxide NPs onto their surfaces. As for the synthesis of metal oxide NPs, mild hydrothermal method has been known as an efficient route and extended to prepare binary and/or ternary transition metal oxide NPs [20–22]. To the best of our knowledge, the synthesis and electrochemical performance of the Ru-based binary oxide NPs dispersed well onto the MWCNTs surfaces have been reported scarcely.

In the work, we first synthesized $\text{Ru}_{0.58}\text{In}_{0.42}\text{O}_y \cdot n\text{H}_2\text{O}/\text{FMWCNTs}$ nanocomposites with uniform structure, where $\text{Ru}_{0.58}\text{In}_{0.42}\text{O}_y \cdot n\text{H}_2\text{O}$ NPs were mono-dispersed onto the FMWCNTs surfaces under mild hydrothermal condition. The unique nanocomposites delivered desirable electrochemical capacitance. And electrochemical performance of a symmetric EC constructed by using the $\text{Ru}_{0.58}\text{In}_{0.42}\text{O}_y \cdot n\text{H}_2\text{O}/\text{FMWCNTs}$ nanocomposites as electrodes was also investigated in detail.

2. Materials and methods

2.1. Materials

MWCNTs were synthesized by the chemical vapor deposition (CVD) method and purified by refluxing them in nitric acid (HNO_3 , 2.6 M) for 12 h before use. All the chemicals used were of analytical grade. $\text{RuCl}_3 \cdot n\text{H}_2\text{O}$, NaCl, absolute ethanol and $\text{InCl}_3 \cdot 4\text{H}_2\text{O}$ were obtained from Nanjing Chemical Company (Nanjing, China). Poly(sodium-4-styrene sulfonate) (average MW, 70,000) was purchased from Aldrich. Saturated calomel electrode (SCE) was manufactured by Leici (Shanghai, China). All aqueous solutions were freshly prepared by using high-purity water (18 M Ω cm resistance) from an Ampeon 1810-B system (Jiangsu, China).

2.2. Synthesis and characterization of $\text{Ru}_{0.58}\text{In}_{0.42}\text{O}_y \cdot n\text{H}_2\text{O}/\text{FMWCNTs}$ nanocomposites and PVA–KOH (5 M)– H_2O gel electrolyte

The FMWCNTs could be obtained by the same method as we reported before [9,11–13]. Then, the obtained FMWCNTs were ultrasonicated into 120 mL water with 35 mg $\text{RuCl}_3 \cdot n\text{H}_2\text{O}$ and certain amount of $\text{InCl}_3 \cdot 4\text{H}_2\text{O}$ with the molar ratio of 3:2 for Ru and In species, which was further ultrasonicated for 0.5 h. After well mixed, the pH of the mixture was adjusted to ca. 5. Then the precursor was kept in a Teflon-lined autoclave (150 mL) with a stainless steel shell. After heated to 180 °C, the autoclave was kept at the temperature for 6 h in an oven and then cooled to room temperature naturally. The reaction product was filtered, washed repeatedly and then dried at 80 °C. The alkaline polymer gel electrolyte (PVA–KOH (5 M)– H_2O) was prepared by the solution-casting technique, as we reported previously [32].

The morphology and structure of the nanocomposites were examined by scanning electron microscopy (SEM, LEO 1430VP, Germany) and transmission electron microscope (TEM) (FEI, TECNAI-20) coupled with an energy dispersive X-ray (EDX) analyzer (Link-200, Britain), and by X-ray diffraction (XRD, Max 18 XCE, Japan) using a Cu K α source.

2.3. Electrochemical tests

Electrodes for electrochemical measurements were prepared by mixed electroactive materials with acetylene black (AB) and polytetrafluoroethylene (PTFE) with the weight ratio of 5:1:0.5. A small amount of water was then added to this composite to form a more homogeneous mixture, which was pressed (12 MPa) onto nickel grid (1 cm²) serving as a current collector. The typical loading of the electroactive material was 5 mg. The electrochemical

performance of the as-prepared $\text{Ru}_{0.58}\text{In}_{0.42}\text{O}_y \cdot n\text{H}_2\text{O}/\text{FMWCNTs}$ nanocomposites was evaluated in 5 M KOH solution. A platinum plate (1 cm²) and a SCE were used as the counter and reference electrodes, respectively. Then, a symmetric EC was constructed by using $\text{Ru}_{0.58}\text{In}_{0.42}\text{O}_y \cdot n\text{H}_2\text{O}/\text{FMWCNTs}$ nanocomposites as electrodes and the alkaline polymer gel electrolyte (PVA–KOH (5 M)– H_2O) as an electrolyte and a spacer [32].

Electrochemical performance was evaluated by cyclic voltammetry (CV) performed by CHI660C electrochemical workstation system. Galvanostatic charge/discharge, leak current and self-discharge tests were carried out with a BT2042 battery tester.

3. Results and discussion

3.1. The characteristics of $\text{Ru}_{0.58}\text{In}_{0.42}\text{O}_y \cdot n\text{H}_2\text{O}/\text{FMWCNTs}$ nanocomposites

Fig. 1 displays the wide-angle XRD pattern of $\text{Ru}_{0.58}\text{In}_{0.42}\text{O}_y \cdot n\text{H}_2\text{O}/\text{FMWCNTs}$ nanocomposites. As indicated by the solid black circles, the diffraction peak at $2\theta = 26.5^\circ$ is identified for the (0 0 2) plane reflection of FMWCNTs [33,34]. Other two obvious peaks with lower intensities at $2\theta = 35.1^\circ$ and 54.4° are ascribed to (1 0 1) and (2 1 1) crystal faces of $\text{RuO}_2 \cdot n\text{H}_2\text{O}$ phase, respectively. Notably, the broad diffraction peaks with lower intensity should result from the relative poor crystalline quality and/or nanometer-scale size of the as-prepared hydrous Ru–In binary oxides NPs. The EDX data presented in the inset reveals the existence of In species in the binary oxides. And the molar ratio of Ru and In species is 0.58–0.42, which is almost the same as that in the precursor solution. Of note, the typical diffraction peaks of In_2O_3 have not been found in Fig. 1. Therefore, the Ru–In binary oxides is a solid solution and donated as $\text{Ru}_{0.58}\text{In}_{0.42}\text{O}_y \cdot n\text{H}_2\text{O}$. The presence of S element reveals the vestige of the PSS in the nanocomposites. The amount of PSS in the nanocomposites can be estimated as ca. 1 wt.% based on the presented EDX data.

The SEM images of the $\text{Ru}_{0.58}\text{In}_{0.42}\text{O}_y \cdot n\text{H}_2\text{O}/\text{FMWCNTs}$ nanocomposites are presented in Fig. 2. From the lower-magnification image (Fig. 2a), the good three-dimensional mesoporous structure with its pores unblocked by the $\text{Ru}_{0.58}\text{In}_{0.42}\text{O}_y \cdot n\text{H}_2\text{O}$ NPs still can be found. Moreover, the obvious coexistence of island-like aggregations of $\text{Ru}_{0.58}\text{In}_{0.42}\text{O}_y \cdot n\text{H}_2\text{O}$ NPs and the bare MWCNTs cannot be seen from the higher-magnification image (Fig. 2b), that is, the $\text{Ru}_{0.58}\text{In}_{0.42}\text{O}_y \cdot n\text{H}_2\text{O}$ NPs are dispersed well onto the FMWCNTs

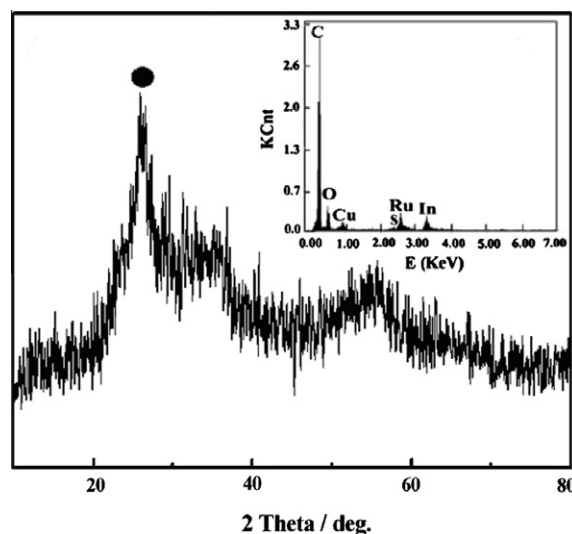


Fig. 1. XRD pattern and EDX (the inset) of $\text{Ru}_{0.58}\text{In}_{0.42}\text{O}_y \cdot n\text{H}_2\text{O}/\text{FMWCNTs}$ nanocomposites.

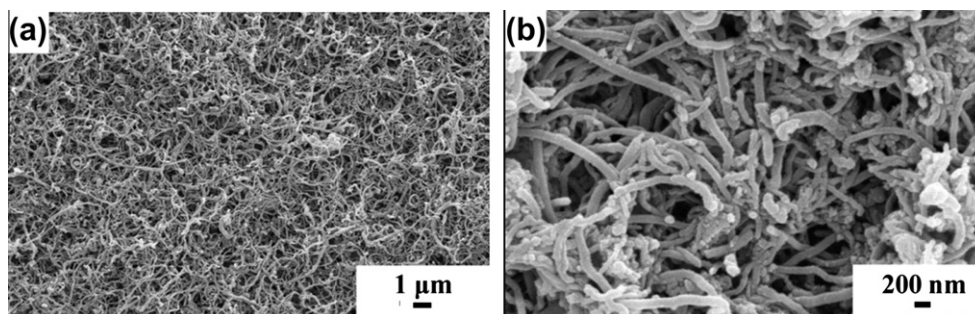


Fig. 2. SEM images (a and b) with different magnification of $\text{Ru}_{0.58}\text{In}_{0.42}\text{O}_y \cdot n\text{H}_2\text{O}/\text{FMWCNTs}$ nanocomposites.

surfaces. To support such viewpoint, TEM images of the nanocomposites are presented in Fig. 3.

Fig. 3 shows the TEM images with different magnification of the $\text{Ru}_{0.58}\text{In}_{0.42}\text{O}_y \cdot n\text{H}_2\text{O}/\text{FMWCNTs}$ nanocomposites. $\text{Ru}_{0.58}\text{In}_{0.42}\text{O}_y \cdot n\text{H}_2\text{O}$ NPs are found to be dispersed well onto the FMWCNTs surfaces, as shown in Fig. 2a, although some clusters (the inset in Fig. 2a) of $\text{Ru}_{0.58}\text{In}_{0.42}\text{O}_y \cdot n\text{H}_2\text{O}$ NPs still exist onto the FMWCNTs surfaces, as indicated by a red ellipse. It indicates that the $\text{Ru}_{0.58}\text{In}_{0.42}\text{O}_y \cdot n\text{H}_2\text{O}$ NPs can be easily attached and mono-dispersed well onto the FMWCNTs surfaces under the hydrothermal condition. As seen from the higher-magnification TEM image (Fig. 2b), the size distribution of $\text{Ru}_{0.58}\text{In}_{0.42}\text{O}_y \cdot n\text{H}_2\text{O}$ NPs dispersed onto the FMWCNTs surfaces is relatively narrow and their average size is ca. 2 nm. The gray of electron diffraction (ED) diffraction rings (the inset in Fig. 2b) reveal a relative poor crystalline quality and/or the nanometer-scale size of the as-synthesized $\text{Ru}_{0.58}\text{In}_{0.42}\text{O}_y \cdot n\text{H}_2\text{O}$ NPs [11,21,35], which is in good agreement with the XRD analysis mentioned above. For comparison, Fig. 4 shows a TEM image of the $\text{Ru}_{0.58}\text{In}_{0.42}\text{O}_y \cdot n\text{H}_2\text{O}/\text{MWCNTs}$ nanocomposites, as expected, a drastic change in dispersity can be observed. The nanoclusters or large aggregations of $\text{Ru}_{0.58}\text{In}_{0.42}\text{O}_y \cdot n\text{H}_2\text{O}$ NPs and the bare MWCNTs randomly co-exist in a mixture when the same procedure is employed just using MWCNTs instead of FMWCNTs. Therefore, PSS plays a great role in the formation of $\text{Ru}_{0.58}\text{In}_{0.42}\text{O}_y \cdot n\text{H}_2\text{O}/\text{FMWCNTs}$ nanocomposites with uniform structure. The solution with the FMWCNTs remains homogeneously ink-like after 1 week or even much longer time, which verifies the good water-solubility and dispersion of FMWCNTs in water. Furthermore, PSS plays a bridging role in increasing the number of active sites for the adsorption, nucleation of Ru–In binary oxide NPs, which would facilitate the heterogeneous growth of the $\text{Ru}_{0.58}\text{In}_{0.42}\text{O}_y \cdot n\text{H}_2\text{O}$ NPs on the FMWCNTs surfaces. For such nanosized and mono-dispersed $\text{Ru}_{0.58}\text{In}_{0.42}\text{O}_y \cdot n\text{H}_2\text{O}$ NPs, good electrochemical capacitance is expected due to the abundant electroactive surface atoms of the $\text{Ru}_{0.58}\text{In}_{0.42}\text{O}_y \cdot n\text{H}_2\text{O}$ NPs, which are contacted easily by the OH^- ions and electrons for efficient energy storage.

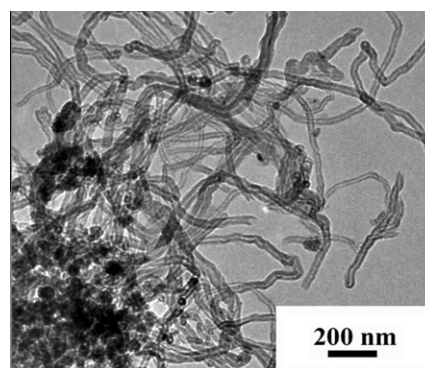


Fig. 4. TEM image of $\text{Ru}_{0.58}\text{In}_{0.42}\text{O}_y \cdot n\text{H}_2\text{O}/\text{MWCNTs}$ nanocomposites.

For such nanosized and mono-dispersed $\text{Ru}_{0.58}\text{In}_{0.42}\text{O}_y \cdot n\text{H}_2\text{O}$ NPs, good electrochemical capacitance is expected due to the abundant electroactive surface atoms of the $\text{Ru}_{0.58}\text{In}_{0.42}\text{O}_y \cdot n\text{H}_2\text{O}$ NPs, which are contacted easily by the OH^- ions and electrons for efficient energy storage.

3.2. Electrochemical behavior of the $\text{Ru}_{0.58}\text{In}_{0.42}\text{O}_y \cdot n\text{H}_2\text{O}/\text{FMWCNTs}$ nanocomposites

Electrochemical performance of the prepared $\text{Ru}_{0.58}\text{In}_{0.42}\text{O}_y \cdot n\text{H}_2\text{O}/\text{FMWCNTs}$ nanocomposites is first investigated in 5 M KOH solution. The typical CV curve at 10 mV s^{-1} of the nanocomposites is shown in Fig. 5a. Obviously, the CV curve of the $\text{Ru}_{0.58}\text{In}_{0.42}\text{O}_y \cdot n\text{H}_2\text{O}/\text{FMWCNTs}$ nanocomposites displays a good rectangular shape with respect to the zero-current line and a rapid current response on voltage reversal at each end potential in the electrochemical window from -1.0 to 0.2 V (vs. SCE). In addition, the electrochemical response current on the positive sweep is mirror-image symmetric to their corresponding counterpart on the negative sweep, revealing good electrochemical capacitance of the nanocomposites in 5 M KOH solution. Comparatively, the CV curve of $\text{Ru}_{0.58}\text{In}_{0.42}\text{O}_y \cdot n\text{H}_2\text{O}/\text{MWCNTs}$ nanocomposites is also plotted in Fig. 5b. The slower current response on voltage reversal at each end potential and the less electrochemical response current both mean that the $\text{Ru}_{0.58}\text{In}_{0.42}\text{O}_y \cdot n\text{H}_2\text{O}/\text{FMWCNTs}$ nanocomposites own much better supercapacitive behavior. Moreover, the obvious redox peaks existing in the CV curves (Fig. 5a and b) suggest the typical pseudocapacitive nature of the nanocomposites for energy storage. The CV plot of FMWCNTs is further depicted in Fig. 5c. Extremely small area under the current–potential curve reveals a very small SC of FMWCNTs themselves. Therefore, the main phase of the nanocomposites for energy storage is the Ru–In binary oxide NPs, rather than the FMWCNTs themselves.

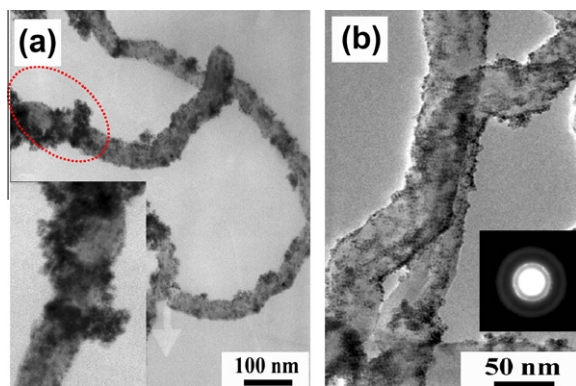


Fig. 3. TEM images (a and b) with different magnification of $\text{Ru}_{0.58}\text{In}_{0.42}\text{O}_y \cdot n\text{H}_2\text{O}/\text{FMWCNTs}$ nanocomposites. The inset in (a) is the magnifying image of the part indicated by the red ellipse and the inset in (b) is the ED pattern of the nanocomposites. (For interpretation of the references to colour in this figure legend, the reader is referred to the web version of this article.)

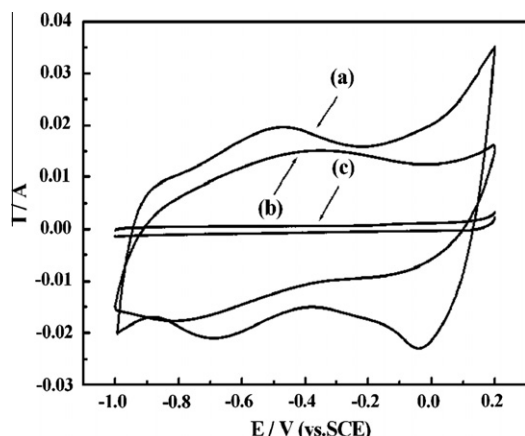


Fig. 5. CV curves (10 mV s^{-1}) of (a) $\text{Ru}_{0.58}\text{In}_{0.42}\text{O}_y \cdot n\text{H}_2\text{O}/\text{FMWCNTs}$ nanocomposites, (b) $\text{Ru}_{0.58}\text{In}_{0.42}\text{O}_y \cdot n\text{H}_2\text{O}/\text{MWCNTs}$ nanocomposites and (c) FMWCNTs.

The voltammetric charge (q) integrated from a positive or negative sweep of CV plots can be used as an effective signal in determining the pseudocapacitance in redox transitions [36]. Accordingly, the average SCs of the electrodes are estimated from the CV curves in Fig. 5, respectively, by integrating the area under the current–potential curve and then dividing by the sweep rate and the potential window according to the following equation:

$$C_{ave} = \frac{q}{vm} = \frac{1}{1.2m\nu} \int_{-1}^{0.2} I(V)dV \quad (1)$$

where ν is a constant of the sweep rate applied for the CV measurements, i.e., dV/dt , $I(V)$ is a current response depending on the sweep voltage, the voltammetric charge is thus estimated as $q = \int_{-1}^{0.2} I(V)dV$, the sweep potential (V) is from -1.0 to 0.2 V and m is the mass of electroactive material in an electrode. The average SC of the $\text{Ru}_{0.58}\text{In}_{0.42}\text{O}_y \cdot n\text{H}_2\text{O}/\text{FMWCNTs}$ nanocomposites can be calculated as *ca.* 319 F g^{-1} , while the SCs of $\text{Ru}_{0.58}\text{In}_{0.42}\text{O}_y \cdot n\text{H}_2\text{O}/\text{MWCNTs}$ nanocomposites and FMWCNTs are just *ca.* 205 and 11 F g^{-1} , respectively, which are much less than $\text{Ru}_{0.58}\text{In}_{0.42}\text{O}_y \cdot n\text{H}_2\text{O}/\text{FMWCNTs}$ nanocomposites.

The good electrochemical performance of the $\text{Ru}_{0.58}\text{In}_{0.42}\text{O}_y \cdot n\text{H}_2\text{O}/\text{FMWCNTs}$ nanocomposites should be related to the good dispersion of the $\text{Ru}_{0.58}\text{In}_{0.42}\text{O}_y \cdot n\text{H}_2\text{O}$ NPs onto the FMWCNTs surfaces, as discussed above. It is well established that nanosized electroactive materials exhibit more attractive properties, such as very small particle size, large exposed surface area, and high surface energy, which can enlarge the contact area, make the best of the electroactive materials and enhance the electrochemical reaction rate [11,21,37,38]. However, the decrease in particle size would increase the inter-particle electron-hopping resistance during the redox transition [39–41] because the number of interface between particles increases with the decrease of particle size. It would be remitted greatly by the introduction of the FMWCNTs with a three-dimensional conducting matrix. Furthermore, FMWCNTs improve the dispersion of $\text{Ru}_{0.58}\text{In}_{0.42}\text{O}_y \cdot n\text{H}_2\text{O}$ NPs, which makes the electroactive $\text{Ru}_{0.58}\text{In}_{0.42}\text{O}_y \cdot n\text{H}_2\text{O}$ NPs accessed by OH^- ions much more easily, and then much more redox reactions take place for energy storage. Thus, the electrochemical utilization of Ru–In binary oxides is improved greatly.

3.3. Electrochemical performance of a symmetric EC constructed by using $\text{Ru}_{0.58}\text{In}_{0.42}\text{O}_y \cdot n\text{H}_2\text{O}/\text{FMWCNTs}$ nanocomposites as electrodes

For the practical application, the electrochemical performance of a symmetric EC based on the as-prepared $\text{Ru}_{0.58}\text{In}_{0.42}\text{O}_y \cdot n\text{H}_2\text{O}/\text{FMWCNTs}$ nanocomposite electrodes is of great significance and

should be considered carefully. Therefore, a quasi-capacitor is assembled by using the $\text{Ru}_{0.58}\text{In}_{0.42}\text{O}_y \cdot n\text{H}_2\text{O}/\text{FMWCNTs}$ nanocomposites as electrodes and the alkaline polymer gel electrolyte (PVA–KOH (5 M)– H_2O) as an electrolyte and a spacer. Its electrochemical behavior in a real two electrode system will be investigated in detail in the next section.

Typical CV curves of the symmetric EC at various sweep rates ranged from 5 to 100 mV s^{-1} are demonstrated in Fig. 6. As seen from Fig. 6, at the lower scan rate (such as, 5 mV s^{-1}), the symmetric EC shows almost ideal rectangular shape, suggesting its good capacitive behavior. The good capacitive performance of the symmetric EC still can be seen when the scan rate increases to 50 mV s^{-1} and even 100 mV s^{-1} , although some deviation from ideal rectangularity of the CV curve can be found.

According to the following equation:

$$C_{ave, cell} = \frac{q}{vm} = \frac{1}{1.3m\nu} \int_0^{1.3} I(V)dV \quad (2)$$

where ν is a constant of the sweep rate applied for the CV measurements, $I(V)$ is a current response depending on the sweep voltage, the sweep potential (V) is from 0 to 1.3 V and m is the total mass of electroactive $\text{Ru}_{0.58}\text{In}_{0.42}\text{O}_y \cdot n\text{H}_2\text{O}/\text{FMWCNTs}$ nanocomposites in the two electrodes. The average SCs of the symmetric EC can be estimated as *ca.* 71 , 67 , 62 F g^{-1} at 5 , 50 , 100 mV s^{-1} , respectively, based on the CV curves in Fig. 6. Notably, the SC at a scan rate of 100 mV s^{-1} is *ca.* 87% of that at 5 mV s^{-1} , revealing the good power and energy properties of the symmetric EC, which is important for its practical application.

The capacitive reversibility and power property of an EC are usually examined by the charge–discharge tests under various current densities [42]. Thereupon, typical chronopotentiometry (CP) curves of the symmetric EC within an electrochemical window ranged from 0.0 to 1.3 V are shown in Fig. 7. The E – t responses behave as symmetric triangular shape during the charge–discharge processes and the potential is linearly dependent on the charge–discharge time after the iR drop, exhibiting its good capacitive behavior. The SC of the symmetric EC could be calculated as follows:

$$C_{m, cell} = \frac{It}{\Delta Vm} \quad (3)$$

where I , t , m and ΔV indicate the constant current, the discharge time, the total electroactive material mass of the two electrodes and the electrochemical window of 1.3 V , respectively. And the SCs of the EC at different current densities are collected and shown in Table 1.

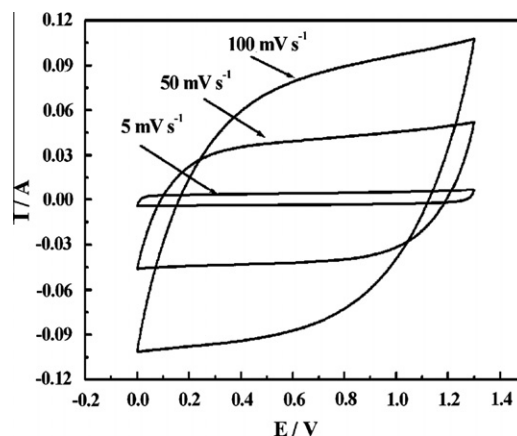


Fig. 6. CV curves of the symmetric EC based on the $\text{Ru}_{0.58}\text{In}_{0.42}\text{O}_y \cdot n\text{H}_2\text{O}/\text{FMWCNTs}$ nanocomposites.

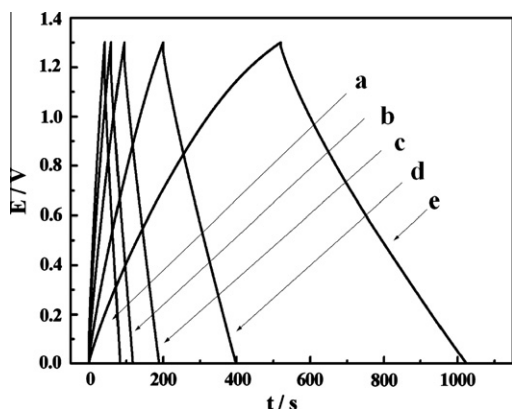


Fig. 7. Constant charge/discharge curves of the symmetric EC based on the $\text{Ru}_{0.58}\text{In}_{0.42}\text{O}_y \cdot n\text{H}_2\text{O}/\text{FMWCNTs}$ nanocomposites: (a) 20 mA cm^{-2} , (b) 15 mA cm^{-2} , (c) 10 mA cm^{-2} , (d) 5 mA cm^{-2} and (e) 2 mA cm^{-2} .

Table 1
Coulomb efficiency and SCs for the symmetric EC at various current densities.

$I \text{ (mA cm}^{-2}\text{)}$	2	5	10	15	20
$\eta \text{ (\%)}$	97.3	98.0	98.4	99.1	99.8
SCs (F g^{-1})	77.1	76.1	74.2	68.9	66.1

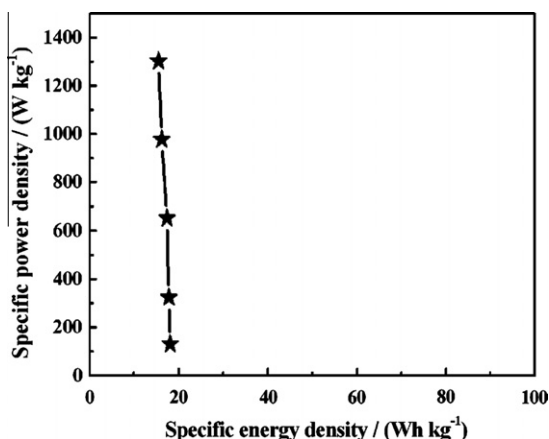


Fig. 8. Ragone plot of the symmetric EC based on the $\text{Ru}_{0.58}\text{In}_{0.42}\text{O}_y \cdot n\text{H}_2\text{O}/\text{FMWCNTs}$ nanocomposites.

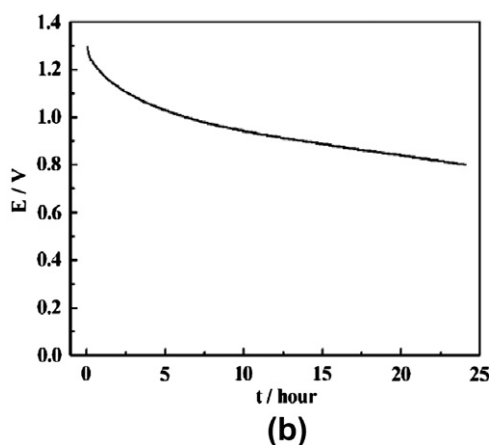
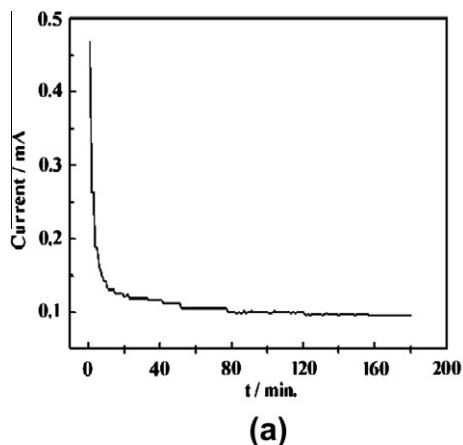


Fig. 9. Leak current plot (a) and self-discharge (b) of the symmetric EC based on the $\text{Ru}_{0.58}\text{In}_{0.42}\text{O}_y \cdot n\text{H}_2\text{O}/\text{FMWCNTs}$ nanocomposites.

From the data collected in Table 1, the SCs of the symmetric EC are generally decreased with the increase of the applied charging/discharging current density. Such phenomenon is often found for carbon-based electrodes [43], which can be attributed to the two aspects: one is the delay in double-layer responses within the pores because of the incomplete structure of electric double layers [44]; and the other is OH^- depletion during the redox transition of Ru–In binary oxides and a significant decrease of ionic conductivity in the electrolyte at a higher current density [45]. However, the SC at 20 mA cm^{-2} still remains above 86% of that at 2 mA cm^{-2} . It further suggests the good rate capability of the symmetric EC.

Coulomb efficiency (η), as another significant parameter during charging/discharging for any energy-storage device, is also calculated for the symmetric EC according to the following equation:

$$\eta = \frac{t_D}{t_C} \times 100 \quad (4)$$

where t_D and t_C are the expressions of discharge and charge time, respectively. The typical results are calculated and collected in Table 1. Clearly, the coulomb efficiencies are all above 97% from 2 to 20 mA cm^{-2} , which further confirms the good reversibility of the symmetric EC.

Ragone plots for batteries are now complemented by those for ECs, especially as the latter are perceived as energy storage systems capable of high power delivery and high-power-level re-charge. Therefore, it is important to qualitatively evaluate the power density (P_{cell}) and energy density (E_{cell}) relationship of the symmetric EC. According to the Eqs. (5) and (6), the E_{cell} and P_{cell} are calculated based on the CP curves in Fig. 7, respectively, and then plotted in Fig. 8.

$$E_{\text{cell}} = \frac{1}{2} C_{\text{m,cell}} (\Delta V)^2 \quad (5)$$

$$P_{\text{cell}} = \frac{E_{\text{cell}}}{t} \quad (6)$$

where $C_{\text{m,cell}}$, ΔV and t are the SC, the maximum electrochemical window, and the discharge time of the symmetric EC, respectively. The Ragone plot is depicted in Fig. 8. Obviously, an E_{cell} of 18.1 Wh kg^{-1} can be delivered at 2 mA cm^{-2} , then decreases to 15.5 Wh kg^{-1} when the current increases up to 20 mA cm^{-2} . However, the P_{cell} can reach 1302 W kg^{-1} at a current density of 20 mA cm^{-2} .

The characteristic of the leakage current and self discharge are another two important aspects for the practical application of ECs. The leakage current of the symmetric EC is measured at 1.3 V floating as shown in Fig. 9a. The current decreases gradually

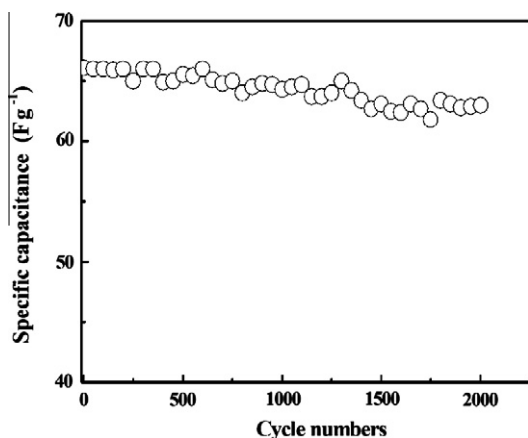


Fig. 10. Cycle life of the symmetric EC based on the $\text{Ru}_{0.58}\text{In}_{0.42}\text{O}_y \cdot n\text{H}_2\text{O}/\text{FMWCNTs}$ nanocomposites.

and remains ca. 0.096 mA after 3 h. The leakage resistant can be evaluated to be $1.35 \times 10^4 \Omega$ by using the following equation:

$$R_p = \frac{V_w}{I_L} \quad (7)$$

where R_p , V_w and I_L are the leakage resistant, the working voltage and the leakage current, respectively. The leakage current is known to be composed of two types of currents [46,47]: the electronic current and the ionic current. The electronic current is mainly ascribed to decomposition of the electrolyte components [46,47]; in fact, the steady-state current ($5 \sim 7 \times 10^{-5}$ A) commonly could be observed after ca. 24 h. On the other hand, the ionic current is due to charging current for the noncharged part of the electrode (corresponding to the high impedance part of the electrode). The ionic current may be predominant in the over-all leak currents within the test period in Fig. 9a, because the steady-state current corresponding to the leak current is low. The leak current is responsible for the self-discharging of the EC. Self-discharge characteristic of the assembled EC is shown in Fig. 9b. The discharging curve is recorded under open circuit condition after constant-current charging to a cell voltage of 1.3 V. The EC shows that the cell voltage still can remain ca. 0.8 V after 24 h.

The long term cyclability is of great importance for electrical vehicle application. Therefore, the cycling behavior of the symmetric EC based on $\text{Ru}_{0.58}\text{In}_{0.42}\text{O}_y \cdot n\text{H}_2\text{O}/\text{FMWCNTs}$ nanocomposites, during charging/discharging at 20 mA cm^{-2} for continuous 2000 cycles without relaxation was performed within the electrochemical window from 0.0 to 1.3 V. As shown in Fig. 10, the SCs of the symmetric EC decrease with the growth of the cycle number. After continuous 2000 cycles, the capacitance value remains ca. 84.7% of that of the first cycle. The capacitance attenuation of 15.3% suggests the good electrochemical stability of the symmetric EC.

4. Conclusions

In conclusion, $\text{Ru}_{0.58}\text{In}_{0.42}\text{O}_y \cdot n\text{H}_2\text{O}$ nanoparticles were first dispersed well onto the poly(sodium-4-styrene sulfonate)-functionalized MWCNTs surfaces under the mild hydrothermal condition. Here, poly(sodium-4-styrene sulfonate) acted as a bifunctional molecule both for solubilizing and dispersing MWCNTs into aqueous solution and further for tethering Ru^{3+} and In^{3+} ions to facilitate the subsequent formation of $\text{Ru}_{0.58}\text{In}_{0.42}\text{O}_y \cdot n\text{H}_2\text{O}$ NPs onto their surfaces. Such unique structure made ions and electrons easily contact much more electroactive sites for sufficient energy storage. Then, a symmetric EC based on the $\text{Ru}_{0.58}\text{In}_{0.42}\text{O}_y \cdot n\text{H}_2\text{O}/\text{FMWCNTs}$ nanocomposites was also presented and delivered good electrochemical capacitance. Furthermore, the method we applied here is versatile and expected to extend to synthesize other Ru-

based binary oxides NPs dispersed well onto the MWCNTs surfaces for ECs application.

Acknowledgments

This work was supported by the National Basic Research Program of China (973 Program) (No. 2007CB209703), the National Natural Science Foundation of China (Nos. 20633040 and 20873064) and 2010 Young Teachers' Research Foundation of Anhui University of Technology (No. QZ201003).

References

- [1] H. Zhang, G.P. Cao, Z.Y. Wang, Y.S. Yang, Z.J. Shi, Z.N. Gu, *Nano Lett.* 8 (2008) 2664.
- [2] M.D. Stoller, S.J. Park, Y.W. Zhu, J. An, R.S. Ruoff, *Nano Lett.* 8 (2008) 3498.
- [3] Y. Wang, Z.Q. Shi, Y. Huang, Y.F. Ma, C.Y. Wang, M.M. Chen, Y.S. Chen, *J. Phys. Chem. C* 113 (2009) 13103.
- [4] D.R. Rolison, J.W. Long, J.C. Lytle, A.E. Fischer, C.P. Rhodes, T.M. McEvoy, M.E. Bourg, A.M. Lubers, *Chem. Soc. Rev.* 38 (2001) 387.
- [5] C.Z. Yuan, B. Gao, L.F. Shen, S.D. Yang, L. Hao, X.J. Lu, F. Zhang, L.J. Zhang, X.G. Zhang, *Nano Scale*, doi: 10.1039/c0nr00423e.
- [6] F. Beguin, K. Szostak, G. Lota, E. Frackowiak, *Adv. Mater.* 17 (2005) 2380.
- [7] E. Frackowiak, S. Delpeux, K. Jurewicz, K. Szostak, D. Cazorla-Amoro, F. Beguin, *Chem. Phys. Lett.* 361 (2002) 35.
- [8] B. Gao, L. Hao, Q.B. Fu, L.H. Su, L.H. Su, C.Z. Yuan, X.G. Zhang, *Electrochim. Acta* 55 (2010) 2311.
- [9] L. Chen, C.Z. Yuan, H. Dou, B. Gao, S.Y. Chen, X.G. Zhang, *Electrochim. Acta* 54 (2009) 2335.
- [10] A. Burke, *J. Power Sources* 91 (2000) 37.
- [11] C.Z. Yuan, L. Chen, B. Gao, L.H. Su, X.G. Zhang, *J. Mater. Chem.* 19 (2009) 246.
- [12] C.Z. Yuan, L.H. Su, B. Gao, X.G. Zhang, *Electrochim. Acta* 53 (2008) 7039.
- [13] C.Z. Yuan, S.L. Xiong, X.G. Zhang, L.F. Shen, F. Zhang, B. Gao, L.H. Su, *Nano Res.* 2 (2009) 722.
- [14] E. Raymundo-Piñero, V. Khomenko, E. Frackowiak, F. Béguin, *J. Electrochem. Soc.* 152 (2005) A229.
- [15] K.X. He, Q.F. Wu, X.G. Zhang, *J. Electrochem. Soc.* 153 (2006) A1568.
- [16] B. Gao, C.Z. Yuan, L.H. Su, S.Y. Chen, X.G. Zhang, *Electrochim. Acta* 54 (2009) 3561–3567.
- [17] N. Krstajić, S. Trasatti, *J. Electrochem. Soc.* 142 (1995) 2675.
- [18] Y. Liu, W.W. Zhao, X.G. Zhang, *Electrochim. Acta* 53 (2008) 3296.
- [19] K. Macounová, I. Jirka, A. Trojānek, M. Makarova, Z. Samec, P. Krtil, *J. Electrochem. Soc.* 154 (2007) A1077.
- [20] C.Z. Yuan, H. Dou, B. Gao, L.H. Su, X.G. Zhang, *J. Solid State Electrochem.* 12 (2008) 1645.
- [21] C.C. Hu, K.H. Chang, C.C. Wang, *Electrochim. Acta* 52 (2007) 4411.
- [22] K.H. Chang, C.C. Hu, *Electrochim. Acta* 52 (2006) 1749.
- [23] C.Z. Yuan, B. Gao, X.G. Zhang, *J. Power Sources* 173 (2007) 606.
- [24] K. Yokoshima, T. Shibutani, M. Hirota, W. Sugimoto, Y. Murakami, Y. Takasu, *J. Power Sources* 160 (2006) 1480.
- [25] B. Gao, X.G. Zhang, C.Z. Yuan, J. Li, L. Yu, *Electrochim. Acta* 52 (2006) 1028.
- [26] Y.U. Jeong, A. Manthiram, *Electrochem. Solid-State Lett.* 3 (2000) 205.
- [27] O.R. Camara, S. Trasatti, *Electrochim. Acta* 41 (1996) 419.
- [28] L.A. Defaria, J.F.C. Boodts, S. Trasatti, *Electrochim. Acta* 37 (1992) 2511.
- [29] K.P. Gong, P. Yu, L. Su, S.X. Xiong, L.Q. Mao, *J. Phys. Chem. C* 111 (2007) 1882.
- [30] J. Chem, H. Liu, W.A. Weimer, M.D. Halls, D.H. Waldeck, G.C. Walker, *J. Am. Chem. Soc.* 124 (2002) 9034.
- [31] S.J. Huang, A.B. Artyukhin, Y.M. Wang, J.W. Ju, P. Stroeve, A. Noy, *J. Am. Chem. Soc.* 127 (2005) 14176.
- [32] C.Z. Yuan, X.G. Zhang, Q.F. Wu, B. Gao, *Solid State Ionics* 177 (2007) 1237.
- [33] Z.S. Lou, Q.W. Chen, W. Wang, Y.F. Zhang, *Carbon* 41 (2003) 3063.
- [34] N. Pierard, A. Fonseca, Z. Konya, I. Willems, G. Van Tendeloo, J.B. Nagy, *Chem. Phys. Lett.* 335 (2001) 1.
- [35] L.R. Hou, C.F. Wang, L. Chen, S. Chen, *J. Mater. Chem.* 2010, doi: 10.1039/b926761a.
- [36] B.E. Conway, *Electrochemical Supercapacitors: Scientific Fundamentals and Technological Applications*, Kluwer Academic/Plenum, New York, 1999.
- [37] F.B. Zhang, Y.K. Zhou, H.L. Li, *Mater. Chem. Phys.* 83 (2004) 260.
- [38] C.Z. Yuan, L.F. Shen, F. Zhang, X.J. Lu, D.K. Li, X.G. Zhang, *J. Colloid. Interface. Sci.* 349 (2010) 181.
- [39] C.C. Hu, W.C. Chen, K.H. Chang, *J. Electrochem. Soc.* 151 (2004) A281–A290.
- [40] C.C. Hu, W.C. Chen, *Electrochim. Acta* 49 (2004) 3469.
- [41] K.E. Swider, C.I. Merzbacher, P.L. Hagans, D.R. Rolison, *Chem. Mater.* 9 (1997) 1248.
- [42] C.C. Wang, C.C. Hu, *Mater. Chem. Phys.* 83 (2004) 289.
- [43] H. Yang, M. Yoshio, K. Isono, R. Kuramoto, *Electrochem. Solid-State Lett.* 5 (2002) A141.
- [44] C. Niu, E.K. Sichel, R. Hoch, D. Moy, H. Tennent, *Appl. Phys. Lett.* 70 (1997) 1480.
- [45] C.C. Hu, C.C. Wang, *Electrochem. Commun.* 4 (2002) 554.
- [46] Y. Matsuda, M. Morita, M. Ishikawa, M. Ihara, *J. Electrochem. Soc.* 140 (1993) L109.
- [47] M. Ishikawa, M. Morita, M. Ihara, Y. Matsuda, *J. Electrochem. Soc.* 141 (1994) 1730.